amphiphilic polymers. Recently, an easy preparation protocol of the pattern film from most polymers dissolved in chloroform was developed. Films were fabricated by the addition of a copolymer (CAP) of dodecylacrylamide and ω-carboxyhexylacrylamide to polymer solution (Nishikawa et al., 2003). Preparation of a honeycomb-patterned film of cellulose nitrate was reported (Govor and Parisi, 2002), but it was difficult to transform it into the corresponding film of regenerated cellulose. Thus, the patterned film would not be suited for the aforementioned applications. An objective of this study was to prepare a patterned film of cellulose, but not cellulose derivatives.

The other patterns, such as stripe and ladder, were also prepared from the solution of volatile organic solvent (Karthaus et al., 1999; Maruyama et al., 1998). However, cellulose itself is not dissolved in such solvents. Therefore, we prepared patterned films from cellulose acetate in chloroform solution, and then the resulting films were readily converted to cellulose-based patterned films by saponification.

In this communication, we show two methods for preparing honeycomb-patterned films as well as a new preparation method for stripe-patterned film.

2. Materials

Cellulose triacetate (CTA) with the degree of substitution of 2.87 and the degree of polymerization of about 290 was kindly supplied by Daicel Chemical, Osaka, Japan. The CTA was dissolved in chloroform, and an insoluble fraction was removed by filtration. The filtrate was evaporated to give a chloroform-dissolved CTA for the following film preparations.

3. Production methods

3.1. Preparation of honeycomb-patterned film by the direct method

In general, the formation of honeycomb pattern is explained as follows. When moist air is blown on the polymer solution, of which the solvent is volatile and water-immiscible, water in the atmosphere condenses and forms microspheres at the air-polymer solution interface due to the decreased temperature resulting from rapid evaporation of the solvent. When using a water-insoluble polymer and an organic solvent, the polymer is adsorbed to the interface between water and polymer solution, and covers the water microspheres. The water microspheres are prevented from collapsing and fusing to each other by the intervening polymer layers. Surface currents due to the convection of the solution and airflow force the water microsphere into a hexagonal close-packed array (Stenzel, 2002). This is the self-organization process. After a complete evaporation of the solvents, the honeycomb pattern appears on a solid substrate. Such patterned films are easily prepared from CAP, and the pore size could be regulated by varying the preparation conditions, such as polymer concentration, solution volume, and humidity (Nishikawa et al., 2003). Furthermore, most polymers dissolved in chloroform can be fabricated to the film by the addition of CAP.

First, we were successful in preparing a honeycomb-patterned film from CTA with CAP. However, no patterned film with uniform pores was obtained. After several attempts, we could prepare it solely from CTA without CAP. The fabrication method is as follows. CTA/chloroform solution (5 mg/ml) was cast on a petri dish (diameter, 9 cm). Moist air was blown on the spread-out polymer solution from a horn-type nozzle. As the solvent gradually evaporated, CTA precipitated as the patterned film. A scanning electron micrograph of the film observed on a Hitachi S-800 is shown in Fig. 1. An average diameter of the patterned film was approximate 3 μm, but the pore size was not uniform. In addition, because CTA was too sensitive to temperature and humidity variations to prepare it reproducibly, an aggregation of water microspheres occurred and a three dimensional multiplayer was often formed. Thus, it was likely to be difficult to reproducibly prepare honeycomb-patterned microporous films having regular arrays.

3.2. Preparation of honeycomb-patterned film by the transcription method

We developed another method for preparing the honeycomb-patterned cellulose film with uniform pore size. That was the transcription method. A mixture of Polycaprolactone and CAP (10:1) in chloroform gave a well-organized honeycomb pattern with the direct method, and its pore size was also regulated by aforementioned variations (Nishikawa et al., 2003). This polymer blend film was used as a first template.

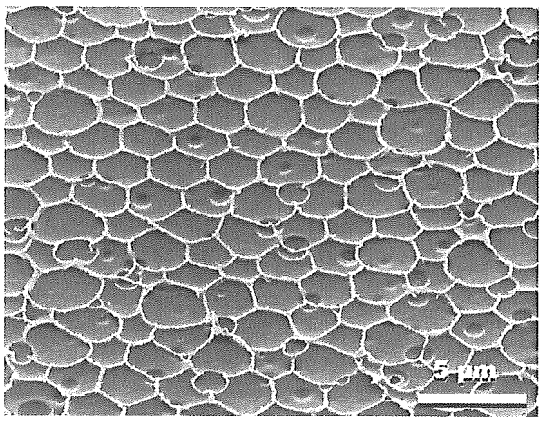

Fig. 1. A scanning electron micrograph of a honeycomb-patterned CTA film prepared by the direct method.

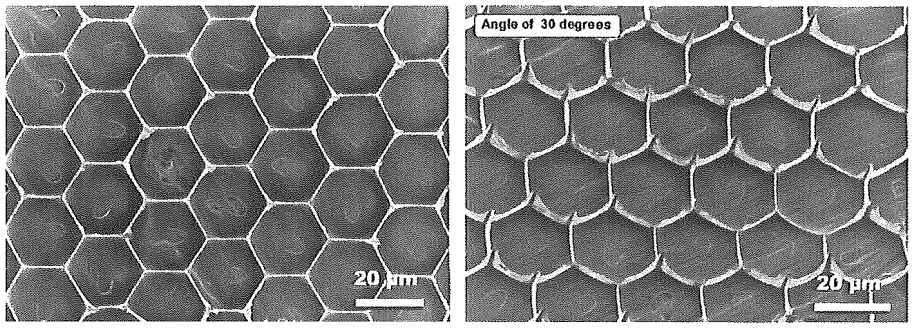

Fig. 2. Scanning electron micrographs of a honeycomb-patterned CTA film prepared by the transcription method.

Poly(dimethyl siloxane) (PDMS) manufactured by Dow Corning Corporation was poured onto the film, and cured with a curing agent for 48 h at room temperature to give a second template after peeling the first template from the second. The PDMS film exhibited the opposite morphology to that of the first template. Its spheres corresponded to the micropores of the honeycomb pattern regularly arrayed on the film. The convex-type of honeycomb pattern was formed, and deep valleys were also formed at the apecies of the hexagons between interfaces of spheres. This result suggests that PDMS effectively penetrates into micropores of the film before curing.

The second template was placed and gently pressed on 0.1 ml of CTA/chloroform solution (5 mg/ml) cast on a glass plate. After evaporating the chloroform, CTA film was peeled from the template to yield a honeycomb-patterned film with well-organized hexagonal micropores, as shown in Fig. 2. Because of the micropores, the surface texture of the supporting material for SEM was observed at the bottom. This indicates that this film can be utilized as a separation membrane. In addition, a structural characteristic of the patterned film fabricated by the transcription method was the presence of pillars at every apex of the hexagons, and the pillars were connected with thin walls. Atomic force microscopic observations showed that the wall and pillar heights were 1.42 μm and 2.80 μm, respectively. The pores look like real cells of honeycomb. This is evidence for CTA penetrating the valleys formed between microspheres of PDMS.

When pressure at the press of second template was low, the resulting film had no micropores because the surface toward the glass plate was covered with CTA. In addition, when CTA/chloroform solution was cast on the second template film followed by evaporation of chloroform, this procedure also resulted in a fine honeycomb-patterned wall, but no micropores. Therefore, these films cannot be used for the aforementioned application.

The patterned CTA films were saponified with sodium methoxide overnight. The FT-IR spectrum of the resulting film using Biorad FTS-50A showed that the carbonyl band at about 1700 cm^{-1} disappeared and the hydroxyl band due to the regeneration of cellulose increased (data not shown). This suggested that a complete saponification was carried out. The morphology of the film did not change during saponification. Clearly, the honeycomb-patterned cellulose film has been fabricated.

3.3. Preparation of stripe-patterned film

When a diluted polymer solution is dropped on a glass plate, the edge of solution moves to the center of the liquid during evaporation of the solvent, resulting in a local gelation of polymer at the edge of the solution on the substrate. By continuous exposure of polymer solution to atmosphere for evaporation of the solvents, the gelation occurred successively, resulting in the formation of ordered mesocopic polymer arrays, such as dots, stripes or ladder patterns (Karthaus et al., 1999; Maruyama et al., 1998).

The stripe-patterned film from CTA/chloroform solution (5 mg/ml) was fabricated by the following procedure. The solution was put between two glass plates. The upper-side glass was pulled horizontally at a speed of 5 mm/min using a motor. The morphology of the resulting film is shown in Fig. 3. Stripes arrayed at a constant space can be observed. In this study, a relation

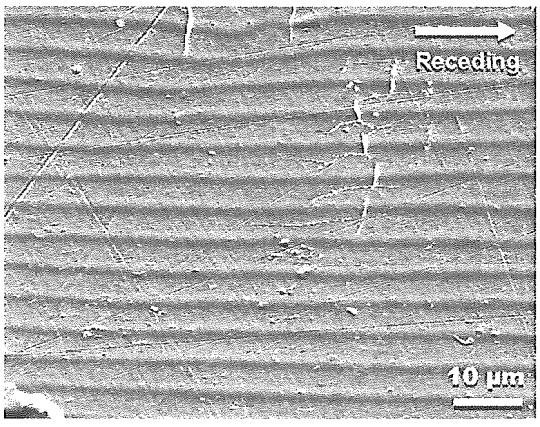

Fig. 3. A scanning electron micrograph of a stripe-patterned CTA film.

between glass moving speed and pattern morphology formed has not been investigated in detail yet.

4. Conclusion

In conclusion, two types of patterned cellulose films were prepared from the corresponding patterned CTA films. The honeycomb-patterned film with well-organized pores was fabricated by the transcription method. Although this transcription method seems to be more tedious and complicated than the direct method, the method has several advantages over the direct method. (1) The patterned PDMS film can be used repeatedly. (2) Preparation conditions, temperature and humidity, do not affect the porous structure of the resulting film, whereas the morphology of the film fabricated by the direct method was too sensitive to the conditions. Therefore, the patterned film can be reproducibly fabricated. (3) Solutions of most polymers, not only in chloroform but also in other solvents, can be used. Therefore, this method can be widely utilized for preparing such films.

A honeycomb pattern was made as a cell culture matrix and as a membrane separation substrate. These methods for preparing patterned arrays due to self-organization are also anticipated as an alternative to lithography for fabricating scaffolds of nano-materials. It is very significant that such materials are produced from cellulose, the "green polymer".

Acknowledgement

This work was financially supported by a Grant-in-Aid for Scientific Research from Japan Society for the Promotion of Science (#15208016).

References

Chen, Y., Pépin, A., 2001. Nanofabrication: Conventional and nonconventional methods. Electrophoresis 22, 187–207.

Govor, L.V., Parisi, J., 2002. Hopping charge transport in honeycomb carbon network structures. Z. Naturforsch. 57a, 757–779.

Imada, M., Noda, S., Chutinan, A., Tokuda, T., Murata, M., Sasaki, G., 1999. Coherent two-dimensional lasing action in surface-emitting laser with triangular-lattice photonic crystal structure. Appl. Phys. Lett. 75, 316–318.

Karthaus, O., Gråsjö, L., Maruyama, N., Shimomura, M., 1999. Formation of ordered mesoscopic polymer arrays by dewetting. Chaos 9, 308–314.

Karthaus, O., Maruyama, N., Yabu, H., Koito, T., Akagi, K., Shimomura, M., 2001. Pattern formation on polymer films by nonlinear processes. Macromol. Symp. 160, 137–142.

Kurono, N., Shimada, R., Ishihara, T., Shimomura, M., 2002. Fabrication and optical property of self-organized honeycomb-patterned film. Mol. Cryst. Liq. Cryst. 377, 285–288.

Maruyama, N., Karthaus, O., Ijiro, K., Shimomura, M., Koito, T., Nishimura, S., Sawadaishi, T., Nishi, N., Tokura, S., 1998. Mesoscopic pattern formation of nanostructured polymer assemblies. Supramol. Sci. 5, 331–336.

Miyamoto, T., Takahashi, S., Ito, H., Inagaki, H., 1989. Tissue biocompatibility of cellulose and its derivatives. J. Biomed. Mater. Res. 23, 125–133.

Nishida, J., Nishikawa, K., Nishimura, S., Wada, S., Karino, T., Nishikawa, T., Ijiro, K., Shimomura, M., 2002. Preparation of self-organized micro-patterned films having cell adhesive ligands. Polym. J. 34, 166–174.

Nishikawa, T., Nonomura, M., Arai, K., Hayashi, J., Sawadaishi, T., Nishiura, Y., Hara, M., Shimomura, M., 2003. Micropatterns based on deformation of a viscoelastic honeycomb mesh. Langmuir 19, 6193–6201.

Risbud, M.V., Bhonde, R.R., 2001. Suitability of cellulose molecular dialysis membrane for bioartificial pancreas: In vitro biocompatibility studies. J. Biomed. Mater. Res. 54, 436–444.

Shimomura, M., Yabu, H., Taguchi, T., 2003. Patent in Japan, JP2003-151766..

Stenzel, M.H., 2002. Formation of regular honeycomb-patterned porous film by self-organization. Aust. J. Chem. 55, 239–243.

Yabu, H., Ijiro, K., Shimomura, M., 2002. Preparation of polymer patterns on wide area. Polym. Prepr. Jpn. 51, 893.

Yabu, H., Tanaka, M., Ijiro, K., Shimomura, M., 2003. Preparation of polyimide honeycomb patterned films by self-organization. Langmuir 19, 6297–6300.

Widawski, G., Rawiso, M., François, B., 1994. Self-organized honeycomb morphology of star-polymer polystyrene films. Nature 369, 387–389.

Wijnhoven, J.E.G.J., Vos, W.L., 1998. Preparation of photonic crystals made of air spheres in titania. Science 281, 802–804.

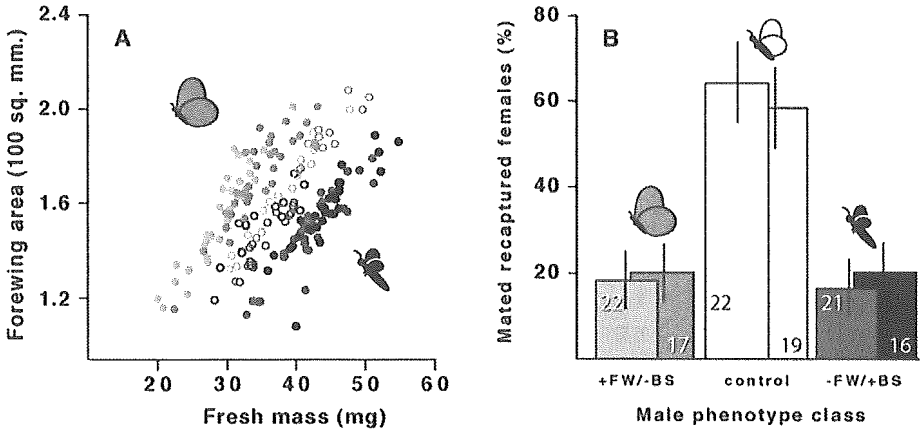

Fig. 4. Distributions of static allometries for FW/BS allometries and relative mating success of three male phenotype classes. (A) Distributions of individual males with +FW/−BM, wild type, and −FW/+BM phenotypes included in the experiment (extreme phenotypes are represented by cartoons). Solid circles denote novel phenotype classes; open circles denote wild-type controls. (B) Mating success of each phenotype class. Columns indicate percentage of recaptured females that mated with males in each class and are shown with 95% confidence intervals based on a bimodal distribution. Numbers in the columns indicate the number of males recaptured in each group. Data from replicate trials are indicated by similar shading (shared between panels).

have documented strong stabilizing selection on male wing loading.

Our findings indicate that it is not internal developmental constraints, but rather external natural selection, that is the primary force shaping the short-term evolution of morphological allometries in insects. However, the surprising bias in the morphological basis of how the allometry evolved suggests that development may strongly influence how individual traits respond to selection on their scaling relationships.

References and Notes

1. D. W. Thompson, *On Growth and Form* (Cambridge Univ. Press, Cambridge, 1917).
2. J. S. Huxley, *Problems of Relative Growth* (Methuen, London, 1932).
3. D. J. Emlen, H. F. Nijhout, *Annu. Rev. Entomol.* **45**, 661 (2000).
4. D. Burkhardt, I. de la Motte, *Entomol. Gen.* **12**, 221 (1987).
5. W. G. Eberhard, E. E. Gutierrez, *Evolution* **45**, 18 (1991).
6. R. E. Strauss, in *Ordination in the Study of Morphology, Evolution, and Systematics of Insects: Applications and Quantitative Genetic Rationales*, J. T. Sorensen, R. Foottit, Eds. (Elsevier Science, Amsterdam, 1992), pp. 157–179.
7. D. J. Emlen, *Science* **291**, 1534 (2001).
8. S. J. Gould, *Biol. Rev.* **41**, 587 (1966).
9. D. L. Stern, D. J. Emlen, *Development* **126**, 1091 (1999).
10. J. Maynard Smith *et al.*, *Q. Rev. Biol.* **60**, 265 (1985).
11. G. P. Wagner, *Am. Zool.* **36**, 36 (1996).
12. G. P. Wagner, G. Booth, H. Bagheri-Chaichian, *Evolution* **51**, 329 (1997).
13. R. Dudley, *The Biomechanics of Insect Flight: Form, Function, Evolution* (Princeton Univ. Press, Princeton, NJ, 2000).
14. S. Vogel, *Comparative Biomechanics* (Princeton Univ. Press, Princeton, NJ, 2003).
15. J. G. Kingsolver, *Evolution* **53**, 1479 (1999).
16. For example, low-flight butterflies such as non-dispersers or perching, sit-and-wait males have lower ratios of flight muscle mass to wing size than do stronger flying butterflies such as dispersing individuals or males that actively patrol for females [reviewed in (*19*)].
17. R. E. Strauss, *Evolution* **44**, 86 (1990).
18. P. Wickman, *Evolution* **46**, 1525 (1992).
19. H. Van Dyck, E. Matthysen, *Trends Ecol. Evol.* **14**, 172 (1999).
20. See supporting data on *Science* Online.
21. R. E. Kooi, P. M. Brakefield, *Entomol. Exp. Appl.* **80**, 149 (1996).
22. D. S. Falconer, T. F. C. MacKay, *Introduction to Quantitative Genetics* (Addison-Wesley Longman, Essex, UK, ed. 4, 1997).
23. D. Schluter, *Evolution* **50**, 1766 (1996).
24. K. E. Weber, *Genetics* **126**, 975 (1990).
25. G. S. Wilkinson, *Genet. Res.* **62**, 213 (1993).
26. D. J. Emlen, *Evolution* **50**, 1219 (1996).
27. J. B. Wolf, W. A. Frankino, A. F. Agrawal, E. D. Brodie III, A. J. Moore, *Evolution* **55**, 232 (2001).
28. S. H. Rice, *Evolution* **52**, 647 (1998).
29. M. Joron, P. M. Brakefield, *Nature* **424**, 191 (2003).
30. R. B. Srygley, J. G. Kingsolver, *Biol. J. Linn. Soc.* **70**, 707 (2000).
31. J. G. Kingsolver, R. B. Srygley, *Evol. Ecol. Res.* **2**, 593 (2000).

32. K. Koops provided essential assistance in rearing caterpillars, with N. Wurzer and colleagues providing maize plants. C. Allen, P. Beldade, and R. Repasky made helpful comments on the manuscript; R. Repasky and A. Buerkle helped with statistics and computer code. In Leiden, we thank R. de Jong and the National Museum of Natural History for access to specimens and the Hortus Botanicus for access to the tropical greenhouse. Supported by Leiden University and by a 2001 NSF Bioinformatics Postdoctoral Fellowship (W.A.F.).

Supporting Online Material

www.sciencemag.org/cgi/content/full/307/5710/718/DC1
Materials and Methods
Figs. S1 and S2
References

20 September 2004; accepted 11 November 2004
10.1126/science.1105409

Mechanisms of Hair Graying: Incomplete Melanocyte Stem Cell Maintenance in the Niche

Emi K. Nishimura,[1]*† Scott R. Granter,[2] David E. Fisher[1]*

Hair graying is the most obvious sign of aging in humans, yet its mechanism is largely unknown. Here, we used melanocyte-tagged transgenic mice and aging human hair follicles to demonstrate that hair graying is caused by defective self-maintenance of melanocyte stem cells. This process is accelerated dramatically with *Bcl2* deficiency, which causes selective apoptosis of melanocyte stem cells, but not of differentiated melanocytes, within the niche at their entry into the dormant state. Furthermore, physiologic aging of melanocyte stem cells was associated with ectopic pigmentation or differentiation within the niche, a process accelerated by mutation of the melanocyte master transcriptional regulator *Mitf*.

Qualitative and quantitative changes in stem and progenitor cells have been implicated in physiological (chronological) aging (*1*, *2*), although the changes are poorly understood and the process of stem-cell aging has not been visually observed. Involvement of stem and progenitor cells in aging of multiple organ systems has been suggested in mice defective in DNA damage repair and telomere maintenance (*3*), but melanocytes may be unique in that the oxidative chemistry of melanin biosynthesis can be cytotoxic (*4*). This led to the suggestion that differentiated, pigmented melanocytes (rather than their unpigmented progenitors) are specifically targeted in hair graying (*5*, *6*). The recent discovery of unpigmented melanocyte stem cells, distinctly located within the hair follicle (*7*), creates an opportunity to determine whether the process of hair graying arises specifically from changes in differentiated melanocytes or the stem-cell pool that provides them.

Stem cells are maintained in the niche microenvironment (*8*). Hair follicles contain a well-demarcated structure for the stem-cell niche (within the lower permanent portion), whereas differentiated melanocytes reside in the hair bulb (at the base of the transient portion of the hair follicle) (Fig. 1A) (*7*, *9*).

Hair follicles are constantly renewing, with alternating phases of growth (anagen), regression (catagen), and rest (telogen) (fig. S1). Taking advantage of the spatial segregation of the stem versus differentiated cell compartments (*7*), we used melanocyte-targeted (Dct) lacZ transgenic mice (*7*, *10*, *11*) to examine the impact of aging on these melanocyte compartments.

Among hair graying models, the melanocyte lineage in *Bcl2*$^{-/-}$ (*12*) and *Mitf*$^{vit/vit}$ (*13*) mice show relatively selective hair graying compared with mouse models of syndromic premature aging, which affect numerous cell lineages (*14*, *15*). Hair graying in the *Bcl2*$^{-/-}$ background has been suggested to arise by chemical cytotoxity of melanin synthesis (*5*, *12*, *16*, *17*). Distribution and morphology of melanoblasts among *Bcl2*$^{-/-}$, *Bcl2*$^{-/+}$, and *Bcl2*$^{+/+}$ mice were normal during early development (fig. S2, a to h). *Bcl2*$^{-/-}$ mice gray after the first hair molting (Fig. 1, B and C) with white hairs. Histologically, differentiated melanocytes were almost completely absent in *Bcl2*$^{-/-}$ pelage (body hair) or whisker follicles (Fig. 1, E and G) compared with *Bcl2*$^{-/+}$ (Fig. 1, D, F, and H) or *Bcl2*$^{+/+}$ (*18*) follicles at postnatal day 39 (P39). Albino background did not protect against melanocyte loss in *Bcl2*$^{-/-}$ mice (Fig. 1I), suggesting that melanin synthesis is unnecessary for this melanocyte disappearance. In addition, *Bcl2*$^{-/-}$ follicles in the second hair cycle lack both differentiated melanocytes in the hair bulb and undifferentiated Dct-lacZ^{+} melanoblasts in the stem-cell niche (located at the bulge area in pelage follicles) (Fig. 1, D and E, and fig. S2, i and j), suggesting that *Bcl2* might be important for survival of melanocyte stem cells.

Looking earlier at P6.5, when hair follicle morphogenesis is almost complete, *Bcl2*$^{-/-}$ follicles appear normal (Fig. 2B). In contrast, *Bcl2*$^{-/-}$ follicles at P8.5 showed sudden, nearly complete loss of melanoblasts in the niche (bulge area, Fig. 2D), whereas the number of melanocytes in the hair bulb did not show significant differences between *Bcl2*$^{-/+}$ and *Bcl2*$^{-/-}$ mice (Fig. 2E). In both pelage and whisker follicles from *Bcl2*$^{-/-}$ animals, disappearance of niche melanoblasts begins at stage 6 of hair follicle morphogenesis [standardized hair follicle stages based on (*19*)], and by stage 8 they are gone (fig. S2, k to n). At this stage, niche melanoblasts undergo a morphologic change from a dendritic shape into a slender, oval shape with shrinkage to maximal nuclear/cytoplasmic ratio upon entry into the dormant state (Fig. 2, F and G). This change in morphology was seen cyclically at corresponding stages of subsequent cycles (*18*). Apoptosis of melanocyte stem cells was observed at the same stage on the albino or black background (*Tyr*$^{c\text{-}2j/c\text{-}2j}$) in both pelage and whisker hair follicles (Fig. 2, H to M). The same pattern of cell loss was detected by using Dct-lacZ, KIT (c-Kit) (KIT), or microphthalmia-associated transcription factor (MITF) as markers (fig. S3 and Fig. 3, A and B). On the other hand, melanocytes in the epidermis and dermis of hairless skin (e.g., tail and soles) survived throughout the hair regeneration cycle (fig. S2, o and p). These findings indicate that BCL2 selectively protects melanocyte stem cells at the time of their transition into the dormant state in the niche and could potentially be responsible for certain forms of human presenile hair graying, although no direct supporting evidence has been reported thus far.

In contrast to *Bcl2*$^{-/-}$, the *Mitf*$^{vit/vit}$ (*13*) graying mouse model exhibited a gradual decrease of melanocyte stem cells rather than abrupt loss (figs. S4 and S6). This strain contains a mild hypomorphic mutation in *Mitf*, the melanocyte master transcriptional regulator [(*20*, *21*) and references therein]. At early to mid-anagen of the third hair cycle, lacZ^{+} cells left in the niche of *Mitf*$^{vit/vit}$ pelage follicles and *Mitf*$^{vit/+}$ whisker follicles often produced melanin pigment and exhibited a bipolar or dendritic morphology (Fig. 3, C and D, and fig. S4, j and s). These pigmented cells are unusual because the niche of wild-type controls contains only unpigmented mel-

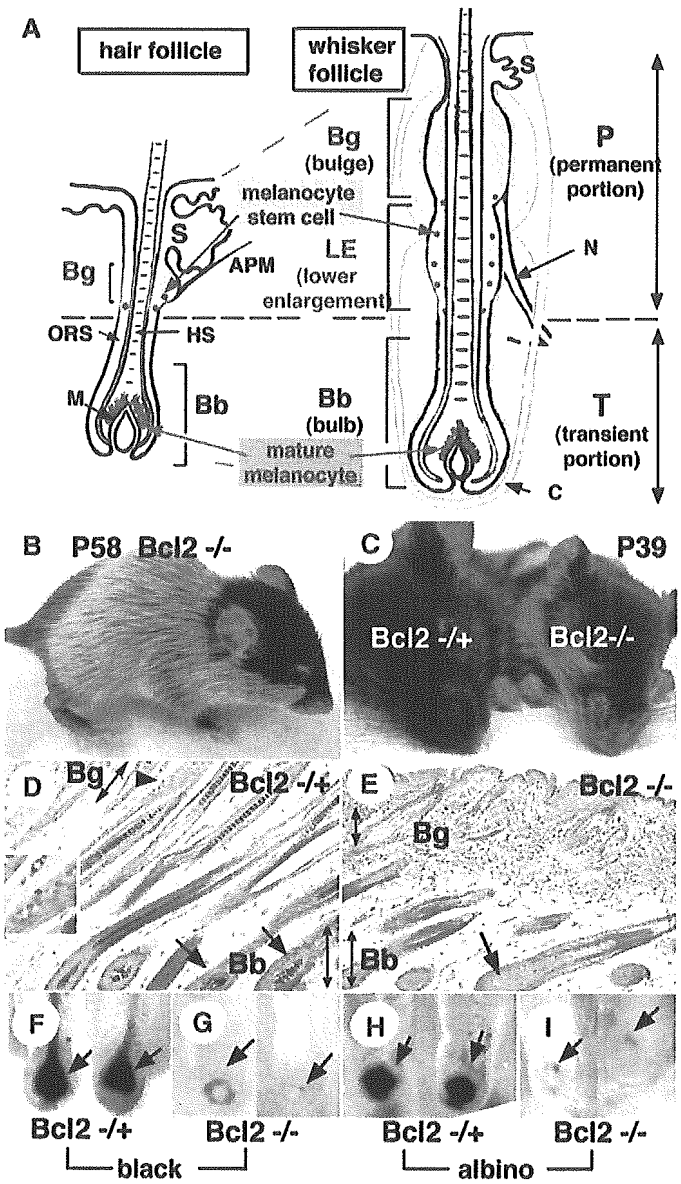

Fig. 1. Differentiated melanocytes are lost in the hair bulb of *Bcl-2* deficient mice. (A) Hair follicle structure. Melanocyte stem cells (blue dots) are in the lower permanent portion (light blue): the bulge (Bg) area in pelage follicles and the lower enlargement (LE) in whisker follicles. APM, arrector pili muscle (Figure 1A legend in SOM). (B) Appearance of *Bcl2*$^{-/-}$ mouse at P58. (C) Hair graying of whiskers in *Bcl2*$^{-/-}$ mouse at P39. (D and E) Distribution of lacZ^{+} cells (melanocytes) in P39 *Bcl2*$^{-/+}$ and *Bcl2*$^{-/-}$ mice carrying the *Dct-lacZ* transgene. Pigmented melanocytes in the bulb (Bb) [arrows in (D)] and lacZ^{+} melanoblasts in the Bg [arrowhead in (D); the inset shows the magnified view] are completely lost in *Bcl2*$^{-/-}$ follicles (E). Double arrows indicate the level of Bb or Bg. Magnification is 100×. (F to I) Whole-mount lacZ staining of the bulb of whisker follicles from *Bcl2*$^{-/+}$ and *Bcl2*$^{-/-}$ in black and white (albino: *Tyr*$^{c\text{-}2j/c\text{-}2j}$) backgrounds at P40. Loss of Dct-lacZ^{+} melanocytes was detected in the bulb of *Bcl2*$^{-/-}$ whisker follicles regardless of albino background.

[1]Department of Pediatric Hematology/Oncology, Melanoma Program in Medical Oncology, Dana-Farber Cancer Institute, Boston Children's Hospital, Harvard Medical School, Boston, MA 02115, USA. [2]Department of Pathology, Brigham and Women's Hospital, Harvard Medical School, Boston, MA 02115, USA.

*To whom correspondence should be addressed. E-mail: emi_k_nishimura@yahoo.co.jp (E.K.N.); David_Fisher@dfci.harvard.edu (D.E.F.)

†Address after 9 February 2005: Department of Dermatology, Hokkaido University Graduate School of Medicine, N15, W7, Sapporo 060-8638, Japan.

anocyte stem cells. We provisionally use the term ectopic pigmentation or differentiation for this reproducibly observed population because it is uncertain by which pathway these cells became pigmented, although they were absent in age-matched controls whose niche melanoblasts remain undifferentiated (Fig. 3E and fig. S4u).

Physiologic (senile) aging in mice also produces hair graying (fig S5), which could be caused by loss of melanocyte stem cells. Indeed during physiologic aging, niche melanoblasts ($lacZ^+$) were lost in a gradual and progressive fashion (Fig. 3, F and G). Moreover, whole-mount cross sections of 8-month-old follicles revealed pigment-containing melanocytes within the stem-cell niche in addition to their scattered distribution in the outer root sheath below the niche in whisker follicles (Fig. 3, H and I, and fig. S5, k to n). The appearance of these pigmented melanocytes in the niche is reminiscent of pigmented niche melanocytes observed during the accelerated graying of *Mitf-vit* mutants. Quantitative analysis revealed that the presence of these cells was accompanied by simultaneous loss of the typical unpigmented Dct-$lacZ^+$ melanoblasts in the niche and correlated closely with aging (Fig. 3, F and G). Thus, self-maintenance of melanocyte stem cells is essentially complete in young animals but becomes defective with aging.

We also analyzed the distribution of melanoblasts in aging human hair follicles with the use of MITF immunostaining (Fig. 4). $MITF^+$ small unpigmented melanoblasts were found in the outer root sheath preferentially around the bulge area where the arrector pili muscle attaches below the level of the sebaceous gland (Fig. 4, A to C), similar to previously described amelanotic melanocytes (*22*, *23*) that express PMEL17 (*24*, *25*), a transcriptional target of MITF (*26*). These cells have been suggested to be a reservoir population for differentiated melanocytes (*23*) and exhibit very similar morphology to melanocyte stem cells in mice. Whereas $MITF^+$ immature melanoblasts were abundant in follicles from 20- to 30-year-old subjects (2 to 3% of the total basal keratinocytes in the bulge area), they were absent from most hair follicles of 70- to 90-year-old subjects (Fig. 4J). $MITF^+$ melanocytes in the uppermost area (infundibulum) of the outer root sheath did not decrease significantly with aging, thus serving as a control population in these studies (fig. S7).

Follicles from intermediate-aged individuals (40 to 60 years old) revealed intermediate loss of bulge melanoblasts (Fig. 4, C and J). Bulge melanoblasts were found more in pigmented follicles than in gray follicles (*18*), as shown recently with $PMEL17^+$ bulge melanoblasts of middle-aged individuals (*27*). In addition, as with aged or $Mitf^{vit}$ mouse follicles, ectopically pigmented $MITF^+$ cells were occasionally observed in the bulge area or just below. These cells closely resembled the dendritic melanocytes described by Narisawa *et al.* in the bulge area of human follicles (*28*). The ectopically pigmented or differentitated melanocytes were seen exclusively in middle-aged follicles but did not accumulate in the bulge area, suggesting that they are not self-maintaining.

Our results demonstrate that *Bcl2* is selectively critical for maintenance of melanocyte stem cells, specifically for entry into the dormant state. *Bcl2* was previously shown to modulate hematopoietic stem-cell pool size (*29*). Different lineages might use distinct antiapoptotic mechanisms to resist the specific stress signals for dormancy.

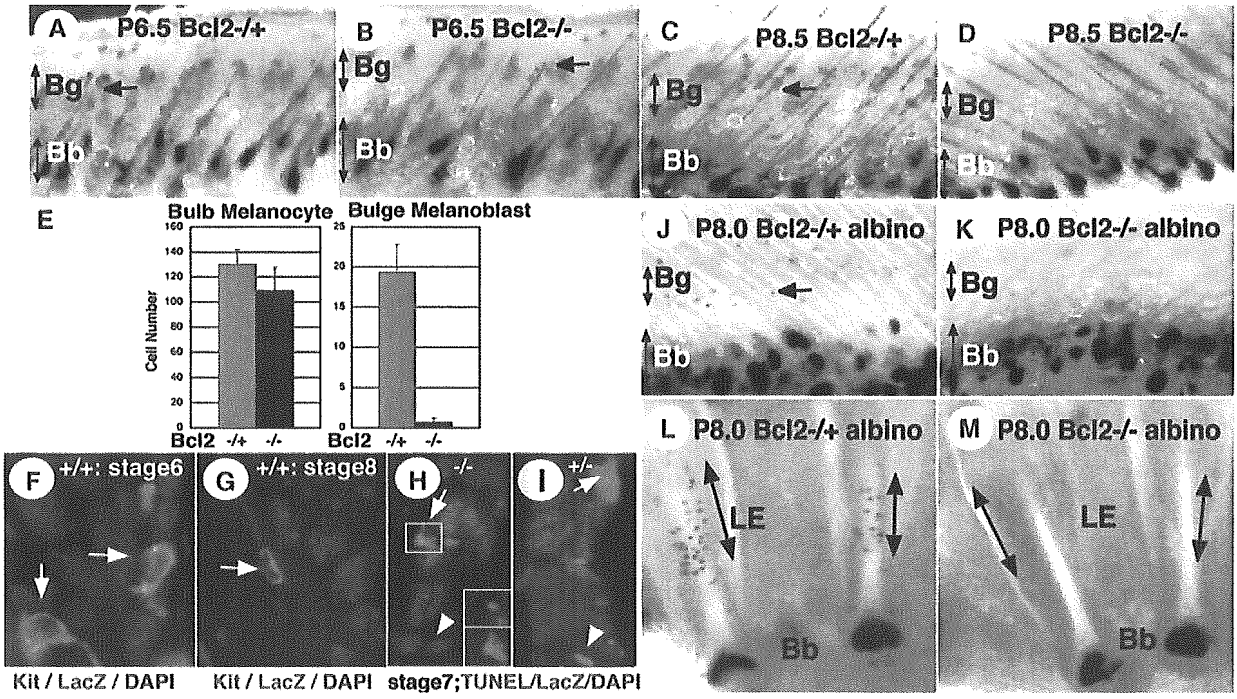

Fig. 2. Loss of $Bcl2^{-/-}$ melanocyte stem cells upon entry into the dormant state. (A to D) Distribution of Dct-$lacZ^+$ melanoblasts (arrows) in the Bg (top double arrow) of pelage follicles at P6.5 and P8.5. Whereas Bb melanocytes appear largely unchanged (bottom double arrow), bulge melanoblasts are lost in $Bcl2^{-/-}$ follicles at P8.5 [compare (D) with (C)] but not at P6.5 [compare (B) with (A)]. (E) Comparison of the total number per field of Dct-$lacZ^+$ melanoblasts in the bulb versus in the bulge plus subbulge of $Bcl2^{-/-}$ and $Bcl2^{-/+}$ pelage follicles at P8.5 on 7-μm sections (magnified 100×). KIT expression matches Dct-$lacZ^+$ in bulge melanoblasts [stage 6 (F) and stage 8 (G)] of $Bcl2^{+/+}$ animals (magnification, 630×). Cell size is diminished from stage 6 to stage 8. Terminal deoxynucleotidyl transferase–mediated deoxyuridine triphosphate nick end labeling (TUNEL), lacZ, and 4′,6′-diamidino-2-phenylindole (DAPI) staining of stage 7 skin from P6.5 $Bcl2^{-/-}$ (H) and P6.5 $Bcl2^{+/-}$ (I) mice. Arrowheads show apoptotic inner root sheath keratinocytes. The inset area, marked with the arrow in (H), shows an apoptotic melanoblast. The top inset on the right shows the merged view for TUNEL (green) and DAPI (blue). The bottom inset shows the merged view for TUNEL (green) and LacZ (red). Distribution of Dct-$lacZ^+$ melanoblasts in the niche: Bg of pelage hair follicles (J and K) and LE (double arrow) of whisker hair follicles [(L and M), double arrows] from P8.0 mice with white backgrounds ($Tyr^{c\text{-}2j/c\text{-}2j}$).

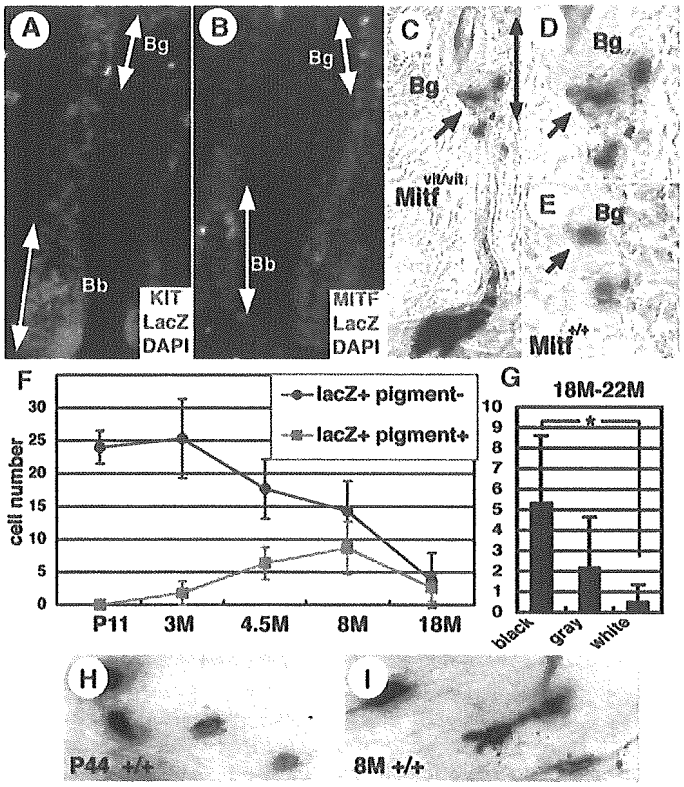

Fig. 3. Effect of aging and *Mitf* mutation on melanocyte stem cells. (**A** and **B**) Coincident expression of Dct-lacZ, KIT, and MITF in hair follicle melanoblasts or melanocytes (magnification, 200×). (See fig. S3 for more details.) (**C**) Ectopically pigmented melanoblasts ($lacZ^+$, blue) in the bulge region (arrow) of 3.5-month-old $Mitf^{vit/vit}$ follicles. (**D**) Magnified view of pigmented bulge melanoblasts. (**E**) Absence of pigment in $lacZ^+$ bulge melanoblasts of age-matched $Mitf^{+/+}$ follicles. (**F**) Quantitation of niche melanocytes ($lacZ^+$), either unpigmented (classical stem cells, blue) or ectopically pigmented (green), in LE of whisker follicles (positions a2 and a3) (see fig. S1i for positions). (**G**) Number of unpigmented niche melanoblasts in whisker follicles (positions a2, a3, c5, and d5) with black, gray, and white hair in 18- to 22-month-old (18–22M) wild-type mice. Asterisk indicates statistical significance ($P < 0.01$). (**H** and **I**) Ectopically pigmented melanoblasts in the niche (LE of whisker follicles) of aging wild-type mice (whole-mount view).

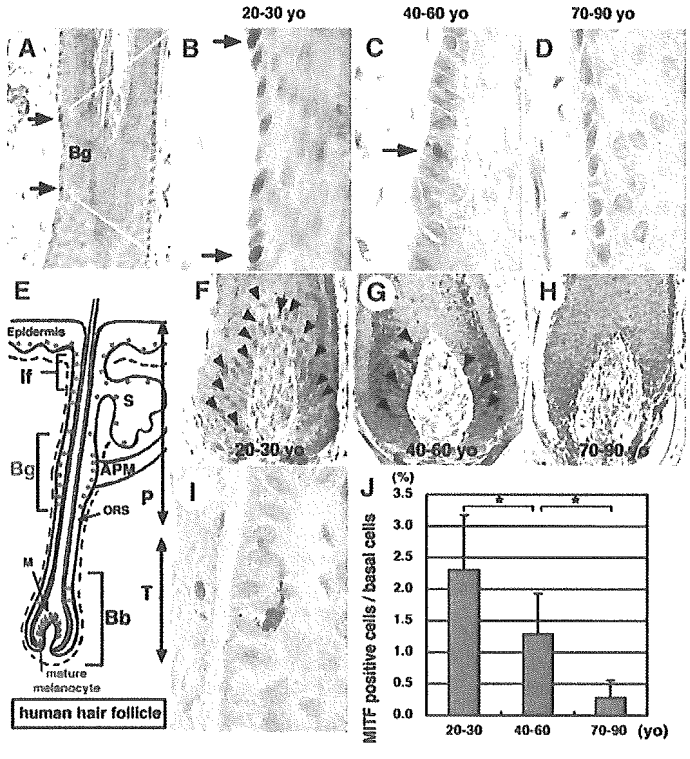

Fig. 4. Melanoblast and melanocyte distribution in human hair follicles from different age groups. Human scalp specimens were immunostained with antibodies against MITF. (**A** and **B**) $MITF^+$ cells (arrows) are distributed on the outer root sheath in the bulge of follicles from 20- to 30-year-old individuals. Magnification in (A), 200×; (B), 630×. (**C** and **D**) Representative views of the bulge from follicles of 40- to 60- and 70- to 90-year-old people, respectively (magnification, 630×). (**E**) Schematic for human hair follicle with pigmented hair. Immature $MITF^{low}$ melanoblasts (blue) are located in the lower permanent portion (the bulge). $MITF^{high}$ melanocytes are located in epidermis, infundibulum (If) (brown), and hair matrix (M, green). ORS, outer root sheath. See Fig. 1A for abbreviations. (**F** to **H**) The bulb region of follicles from different age groups. Mature melanocytes in the hair matrix express MITF (arrowheads). yo, years old. (**I**) An $MITF^+$ melanocyte that contains abundant melanin granules and long dendrites is detected in the bulge and subbulge of follicles specifically from middle-aged individuals. (**J**) The frequency of $MITF^+$ cells per basal keratinocytes in the bulge. Asterisks indicate statistical significance ($P < 0.01$).

Although melanin biosynthesis has been elegantly shown to be cytotoxic in the context of a certain genetic mutation (*6*), stem-cell disappearance in *Bcl2* null mice does not require melanogenesis. *Bcl2* is a transcriptional target of MITF (*30*), but *Bcl2* does not appear to fully account for melanocyte loss in the context of the weakly hypomorphic $Mitf^{vit/vit}$ allele.

Our data suggest a previously unknown pathophysiologic explanation for hair graying. Loss of melanocyte stem cells can be observed and temporally precedes the loss of differentiated melanocytes in the hair matrix. Thus, incomplete maintenance of melanocyte stem cells appears to cause physiologic hair graying through loss of the differentiated progeny with aging. This is associated with ectopic melanocyte pigmentation or differentiation within the niche. Possible explanations include premature differentiation or activation of a senescence program [which induces pigmentation in vitro (*31*)]. Acceleration of this process in $Mitf^{vit}$ follicles implicates MITF in the self-renewal of melanocyte stem cells. The precise roles for stem-cell apoptosis versus ectopic differentiation remain to be determined but may similarly contribute to stem-cell loss in other aging organ systems.

References and Notes

1. M. A. Sussman, P. Anversa, *Annu. Rev. Physiol.* **66**, 29 (2004).
2. G. Van Zant, Y. Liang, *Exp. Hematol.* **31**, 659 (2003).
3. K. K. Wong *et al.*, *Nature* **421**, 643 (2003).
4. K. Urabe *et al.*, *Biochim. Biophys. Acta* **1221**, 272 (1994).
5. J. P. Ortonne, J. J. Nordlund, in *The Pigmentary System*, J. J. Nordlund, R. Boissy, V. J. Hearing, R. King, J. P. Ortonne, Eds. (Oxford Univ. Press, New York, 1998), pp. 489–502.
6. R. Johnson, I. J. Jackson, *Nature Genet.* **1**, 226 (1992).
7. E. K. Nishimura *et al.*, *Nature* **416**, 854 (2002).
8. F. M. Watt, B. L. M. Hogan, *Science* **287**, 1427 (2000).
9. E. Fuchs, B. J. Merrill, C. Jamora, R. DasGupta, *Dev. Cell* **1**, 13 (2001).
10. M. A. Mackenzie, S. A. Jordan, P. S. Budd, I. J. Jackson, *Dev. Biol.* **192**, 99 (1997).
11. K. R. Fitch *et al.*, *Genes Dev.* **17**, 214 (2003).
12. D. J. Veis, C. M. Sorenson, J. R. Shutter, S. J. Korsmeyer, *Cell* **75**, 229 (1993).
13. A. B. Lerner *et al.*, *J. Invest. Dermatol.* **87**, 299 (1986).
14. K. L. Rudolph *et al.*, *Cell* **96**, 701 (1999).
15. J. de Boer *et al.*, *Science* **296**, 1276 (2002); published online 11 April 2002 (10.1126/science.1070174).
16. K. Yamamura *et al.*, *Cancer Res.* **56**, 3546 (1996).
17. D. J. Tobin, R. Paus, *Exp. Gerontol.* **36**, 29 (2001).
18. E. K. Nishimura, S. R. Granter, D. E. Fisher, unpublished data.
19. R. Paus *et al.*, *J. Invest. Dermatol.* **113**, 523 (1999).
20. E. Steingrimsson, N. G. Copeland, N. A. Jenkins, *Annu. Rev. Genet.* **38**, 365 (2004).
21. E. R. Price, D. E. Fisher, *Neuron* **30**, 15 (2001).
22. W. Montagna, H. B. Chase, *Am. J. Anat.* **99**, 415 (1956).
23. R. G. Staricco, *Ann. N. Y. Acad. Sci.* **100**, 239 (1963).
24. T. Horikawa *et al.*, *J. Invest. Dermatol.* **106**, 28 (1996).
25. S. Commo, B. A. Bernard, *Pigment Cell Res.* **13**, 253 (2000).
26. J. Du *et al.*, *Am. J. Pathol.* **163**, 333 (2003).
27. S. Commo, O. Gaillard, B. A. Bernard, *Br. J. Dermatol.* **150**, 435 (2004).
28. Y. Narisawa, H. Kohda, T. Tanaka, *Acta Derm. Venereol.* **77**, 97 (1997).

29. J. Domen, S. H. Cheshier, I. L. Weissman, *J. Exp. Med.* **191**, 253 (2000).
30. G. G. McGill *et al.*, *Cell* **109**, 707 (2002).
31. E. E. Medrano *et al.*, *Mol. Biol. Cell* **5**, 497 (1994).
32. We thank V. Igras and C. Quigley for technical assistance; L. Lamoreux for supplying *Mitf*^{vit} mice; A. Miller, C. Hershey, and Y. Choi for critical reading of the manuscript; members of the Fisher laboratory for helpful discussions; and D. Rowitch for sharing microscopes. E.K.N. wishes to thank Y. Miyachi for continuous encouragement and support. E.K.N. was supported by the Shiseido Award in 2002 and the Charles A. King Trust, Fleet National Bank, a Bank of America Company, co-trustee (Boston, MA). Supported by grant no. AR43369 from NIH to D.E.F. D.E.F. is the Nirenberg Fellow in pediatric oncology at Dana-Farber Cancer Institute.

Supporting Online Material
www.sciencemag.org/cgi/content/full/1099593/DC1
Materials and Methods
Figs. S1 to S7

26 April 2004; accepted 8 December 2004
Published online 23 December 2004;
10.1126/science.1099593
Include this information when citing this paper.

Dynamic Complex Formation During the Yeast Cell Cycle

Ulrik de Lichtenberg,[1]* Lars Juhl Jensen,[2]* Søren Brunak,[1] Peer Bork[2,3]†

To analyze the dynamics of protein complexes during the yeast cell cycle, we integrated data on protein interactions and gene expression. The resulting time-dependent interaction network places both periodically and constitutively expressed proteins in a temporal cell cycle context, thereby revealing previously unknown components and modules. We discovered that most complexes consist of both periodically and constitutively expressed subunits, which suggests that the former control complex activity by a mechanism of just-in-time assembly. Consistent with this, we show that additional regulation through targeted degradation and phosphorylation by Cdc28p (Cdk1) specifically affects the periodically expressed proteins.

Most research on biological networks has been focused on static topological properties (*1*), describing networks as collections of nodes and edges rather than as dynamic structural entities. Here we focus on the temporal aspects of networks, which allows us to study the dynamics of protein complex assembly during the *Saccharomyces cerevisiae* cell cycle.

Our integrative approach combines protein-protein interactions with information on the timing of the transcription of specific genes during the cell cycle, obtained from DNA microarray time series (*2*, *3*). From the latter, we derived a quality-controlled set of 600 periodically expressed genes, each assigned to the point in the cell cycle where its expression peaks (*4*). We then constructed a physical interaction network for the corresponding proteins from yeast two-hybrid screens (*5*, *6*), complex pull-downs (*7*, *8*), and curated complexes from the Munich Information Center for Protein Sequences (MIPS) database (*9*). To reduce the error rate of 30 to 50% expected in most current large-scale interaction screens (*10*, *11*), all physical interaction data were combined, a topology-based confidence score was assigned to each individual interaction [as in the STRING database (*12*)], and only high-confidence interactions were selected (*13*). These were further filtered with information on subcellular localization (*14*) to exclude interactions between proteins annotated to incompatible compartments (*13*); no curated MIPS interactions were lost because of this filtering. The topology-based scoring scheme, filtering, and extraction criteria reduced the error rate for interactions by an order of magnitude to only 3 to 5% (*13*).

In the extracted network (Fig. 1), we included, in addition to the periodically expressed ("dynamic") proteins, constitutively expressed ("static") proteins that preferentially interact with dynamic ones (*13*). The resulting network consists of 300 proteins (Fig. 1, inside circle), including 184 dynamic proteins (colored according to their time of peak expression) and 116 static proteins (depicted in white). For 412 of the 600 dynamic proteins identified in the microarray analysis, no physical interactions of sufficient reliability could be found (Fig. 1, outside circle). Some may be missed subunits of stable complexes already in the network; the majority, however, probably participate in transient interactions, which are often not detected by current interaction assays (*15*).

Although our procedure for extracting interactions might miss some cellular processes that are dominated by transient interactions, most of the stable complexes should have been captured at least partially. Tandem affinity purifications alone should identify at least half of the subunits for 87% of the known yeast complexes (*7*). Compared with the known cell cycle complexes and functional modules (*9*), we found that all but two of them were identified by our approach (better than random at $P < 10^{-30}$). The only exceptions were the anaphase-promoting complex (APC), which can only be detected with a less stringent interaction cutoff, and the Skp1p/Cullin/F-box protein complex (SCF), which appears to be the only cell cycle–related protein complex without a periodically expressed subunit. For completeness, these two complexes were added to the network. Our extraction procedure produces comparable results even if the curated MIPS complexes are excluded entirely from the analysis or if the specific extraction criteria are changed, showing that the method is robust and has much higher coverage than methods of comparable accuracy (*13*).

The derived cell cycle network (Fig. 1, inside circle) contains 29 heavily intraconnected modules; that is, complexes or groups of complex variants that exist at different time points during the yeast cell cycle. In addition to rediscovering many known cell cycle modules, our approach enables us to place more than 30 poorly characterized proteins in the cell cycle network and to predict new unexpected cell cycle contexts for other proteins (*13*). The network contains 31 isolated binary complexes, many of which involve proteins of unknown function, such as Yml119p and Yll032p, which interact and are both putative Cdc28p substrates (*16*) expressed close in time in G_2 phase (*13*).

As an example of the value of combining temporal data with protein-protein interactions, the network reveals a binary complex consisting of the uncharacterized proteins Ymr295p and Ydr348p. Because only Ydr295p is dynamic, the static protein Ydr348p can only be identified as a cell cycle–relevant protein and placed temporally through the integration of the two complementary data types. Indeed, Ydr348p is a putative Cdc28p target (*16*), and the interaction is further supported by the observation that both proteins localize to the bud neck (*14*). Virtually all complexes contain both dynamic and static subunits (Fig. 1), the latter accounting for about half of the direct interaction partners of periodically regulated proteins through all phases of the cell cycle (Fig. 2). Transcriptional regulation thus influences almost all cell cycle complexes and thereby, indirectly, their static subunits. This implies that many cell cycle proteins cannot be identified through the analysis of any sin-

[1]Center for Biological Sequence Analysis, Technical University of Denmark, DK-2800 Lyngby, Denmark. [2]European Molecular Biology Laboratory, D-69117 Heidelberg, Germany. [3]Max-Delbrück-Centre for Molecular Medicine, D-13092 Berlin, Germany.

*These authors contributed equally to this work.
†To whom correspondence should be addressed. E-mail: bork@embl.de

J. Biomater. Sci. Polymer Edn, Vol. 16, No. 5, pp. 549–561 (2005)

Also available online - www.vsppub.com

In vivo degradability of hydrogels prepared from different gelatins by various cross-linking methods

MAKOTO OZEKI and YASUHIKO TABATA *

Institute for Frontier Medical Sciences, Kyoto University, 53 Kawara-cho, Shogoin, Sakyo-ku, Kyoto 606-8507, Japan

Received 25 March 2004; accepted 3 August 2004

Abstract—This study is an investigation to evaluate the *in vivo* degradation of gelatin hydrogels in terms of their number of cross-links. Various hydrogels were prepared from acidic gelatin, extracted from bovine bone, porcine skin or fish scale, and basic gelatin, extracted from porcine skin, through four types of cross-linking methods, i.e., glutaraldehyde (GA) or dehydrothermal treatment and ultraviolet (UV) or electron beam irradiation. The water content of hydrogels and their number of cross-links, calculated from the tensile modulus of hydrogels, were evaluated as the measure of hydrogel cross-linking extent. Following subcutaneous implantation of ^{125}I-labeled gelatin hydrogels into mice, the radioactivity remaining was measured at different time intervals to assess the *in vivo* degradability of hydrogels. Irrespective of the gelatin type and cross-linking method, a good correlation was found between the *in vivo* degradability of hydrogels and their number of cross-links, which is different from the correlation to their water content. This finding indicates that the degradability of hydrogels is governed by their number of cross-links.

Key words: Hydrogel; gelatin; degradability *in vivo*; cross-linking; irradiation.

INTRODUCTION

Growth factors have been widely recognized to act on different types of cells in the body to regulate their proliferation and differentiation by which tissue regeneration is promoted [1]. However, if a growth factor is administered to the body in the solution form, the *in vivo* efficacy of tissue regeneration cannot be always expected because the factor has only a short half-life period. Therefore, it is necessary to develop a drug-delivery system which facilitates the controlled release of growth factors over an extended time period [2, 3].

*To whom correspondence should be addressed. Tel.: (81-75) 751-4121. Fax: (81-75) 751-4646. E-mail: yasuhiko@frontier.kyoto-u.ac.jp

We have explored gelatin hydrogels as delivery system to succeed in the controlled release of biologically active growth factors [3]. Gelatin has been extensively utilized for pharmaceutical and medical purposes. Its biosafety has been proven in various clinical applications over the years [4–6]. For example, it has been used as hard and soft drug capsule [7, 8], sealant for vascular prostheses [9–11] and hemostatic [12–14]. Moreover, gelatin has been studied as a of drug-delivery carrier in the water-soluble [15, 16] or hydrogel form [17–19]. Another advantage of gelatin is the commercial availability of materials with different electric charges [3, 20, 21]. Gelatin is a biodegradable protein prepared by the acid and alkaline processes of collagen. This process allows collagen to denature and change the electrical nature, which provides various types of gelatin with different isoelectric points (IEPs).

We have already demonstrated that the hydrogel prepared from 'acidic' gelatin with IEP 5.0 can release biologically active basic fibroblast growth factor (bFGF) [22, 23], transforming growth factor (TGF)-β1 [24, 25] and hepatocyte growth factor (HGF) *in vivo* [26]. On the other hand, bone morphogenetic protein (BMP)-2 could be released *in vivo* from the hydrogel of 'basic' gelatin with IEP 9.0 [27]. The time period of growth factors remaining in the hydrogels was in good accordance with that of hydrogel remaining, indicating the release mechanism that the growth factor is released accompanied with hydrogel degradation [2, 3, 23]. The *in vivo* degradability of gelatin hydrogels depended on their water content which could be modified by changing the preparation conditions. The hydrogel with higher water contents was degraded for a shorter time period, while the time period of hydrogel degradation became longer with a decrease in the hydrogel water content [22–24, 26, 27].

In this study, hydrogels were prepared from different kinds of gelatin through various cross-linking methods. As a measure of the cross-linking extent of hydrogels, tensile tests were done to calculate the number of hydrogel cross-links, while their water content was also determined. Following implantation of ^{125}I-labeled gelatin hydrogels into the back subcutis of mice, the time profile of radioactivity remaining was evaluated. We examined the relationship between the *in vivo* degradability of hydrogels and their two types of cross-linking measure, such as the water content and the number of cross-links of hydrogels.

MATERIALS AND METHODS

Materials

Gelatin samples with an IEP of 5.0 (MW 99×10^3), prepared by an alkaline process, of the bovine bone, porcine skin and fish scale collagens, or that with an IEP of 9.0 (Mw 99×10^3), prepared through an acidic process, of the porcine skin collagen, were kindly supplied by Nitta Gelatin (Osaka, Japan) and named 'acidic' and 'basic' gelatins, respectively. N′-succinimidyl-3-(4-hydroxy-3,5-di [^{125}I]iodophenyl)propionate ([^{125}I]Bolton-Hunter reagent, NEX-120H, 147 MBq/ml

in anhydrous benzene) was purchased from Perkin-Elmer Life Sciences (Boston, MA, USA). Other chemicals were purchased from Wako Pure Chemical (Kyoto, Japan) and used without further purification.

Preparation of gelatin hydrogels cross-linked by glutaraldehyde treatment

An aqueous solution of 10 wt% gelatin (800 μl) was cast into a polypropylene mold (2 $\times$ 2 cm^2), followed by storage at 4°C for 24 h to allow gelatin to set. The gelled gelatin was placed at 4°C in aqueous solution containing 12.4 μg/ml of glutaraldehyde (GA) and cross-linking reaction was allowed to proceed at 4°C for different time periods. The resulting hydrogel sheet was immersed in 100 mM of glycine aqueous solution for 1 h to block residual aldehyde groups of GA. The hydrogel sheets were rinsed 3 times with double distilled water (DDW) at 4°C and stored in DDW at 4°C until use or assay.

Preparation of gelatin hydrogels cross-linked by dehydrothermal treatment

Non-cross-linked gelatin hydrogels, prepared by the same procedure described before, were freeze-dried. The resulting freeze-dried gelatin hydrogel sheets were cross-linked by dehydrothermal treatment at 140°C for 24, 48 and 72 h in vacuum. The hydrogel sheets were swollen in DDW at 37°C for 24 h until equilibrium was reached. The gelatin hydrogel sheets were stored in DDW at 4°C until use or assay.

Preparation of gelatin hydrogels crosslinked by ultraviolet irradiation

Freeze-dried non-cross-linked gelatin hydrogels were prepared as described above. The resulting freeze-dried gelatin hydrogel sheets were cross-linked by dehydrothermal treatment at 140°C for 48 h in vacuum. Further cross-linking was introduced by ultraviolet (UV) irradiation to both sides of gelatin hydrogel sheets in a Funa-UV-Linker FS-800 (5 $\times$ 8 W, Funakoshi, Tokyo, Japan) for 10, 20 and 30 min. The hydrogels sheets were swollen in DDW at 37°C for 24 h and stored in DDW at 4°C until use or assay.

Preparation of gelatin hydrogels cross-linked by electron beam irradiation

An aqueous solution of 10 wt% gelatin was cast into a polypropylene mold to give a solution depth of 200 μm. The solution was irradiated by different doses (20, 60 and 100 kGy) of electron beam in an Curetron® Electron Beam Processing System (Nissin High Voltage, Tokyo, Japan). The casting and irradiation operation was repeated five times to obtain 1-mm-thick gelatin hydrogels. The resulting gelatin hydrogel sheets were swollen in DDW at 37°C for 24 h to reach the equilibrium and stored in DDW at 4°C until use or assay.

Evaluation of cross-linking extent of gelatin hydrogels

Two measures to evaluate the extent of hydrogel cross-linking were performed. Gelatin hydrogels, cut with scissors to obtain square sheets ($5 \times 5 \times 1$ mm^3) were swollen in DDW and dried at 60°C under vacuum. The weight of hydrogel sheets before and after drying was measured and the weight ratio of water present in the hydrogel to the DDW-swollen hydrogel was calculated as the water content. The cross-linking density was estimated on the basis of the theory of rubber elasticity [28]. The specimens of gelatin hydrogel, with a length of 20 mm, a central width of 10 mm and a thickness of 1 mm, were subjected to a tensile testing on an AGS-5D Autograph (Shimadzu, Kyoto, Japan) with a low capacity load cell (10 N). The initial slope of the stress–strain curve was calculated from the curve of tensile test to obtain the number of cross-links per gelatin molecule by the following equation on the assumption of an affine deformation

$$N = \frac{2\sigma M}{\rho_g v^{1/3} kT(\alpha - \alpha^{-2})},$$

where N is the number of cross-links per gelatin molecule, ρ_g is the density of gelatin, v is the volume fraction of gelatin in hydrogel, M is the molecular weight of gelatin (99×10^3), k is the Boltzmann constant, T is the absolute temperature, σ is the stress (the applied force per unit area of swollen, unstrained hydrogel) and α is the strain determined by the ratio of sample length at tension to initial length of sample [28, 29]. Four hydrogel sheets were used for each hydrogel type. Figure 1 shows the plots of σ *vs.* $(\alpha - \alpha^{-2})$ on gelatin hydrogel cross-linked by dehydrothermal treatment for 24 h. The number of cross-links per gelatin molecule was calculated from the slope of the σ *vs.* $(\alpha - \alpha^{-2})$ plots.

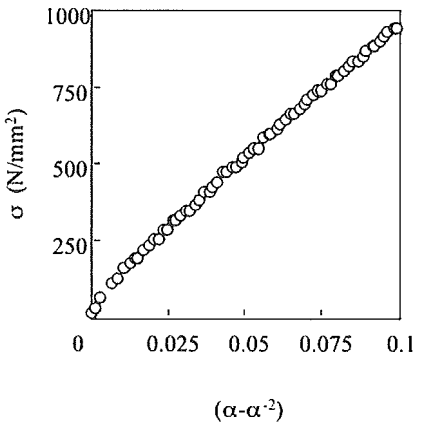

Figure 1. σ *vs.* $(\alpha - \alpha^{-2})$ plots of the gelatin hydrogel cross-linked by dehydrothermal treatment for 24 h.

Radiolabeling of gelatin hydrogels

Gelatin hydrogels were cut with scissors to obtain square sheets ($5 \times 5 \times 1$ mm^3) for the assessment of biodegradability. Gelatin hydrogel sheets were radioiodinated by use of [^{125}I]Bolton-Hunter reagent [30]. Briefly, 20 μl of [^{125}I]Bolton-Hunter reagent solution in anhydrous benzene was bubbled with dry nitrogen gas until benzene was completely evaporated. Then, 1 ml of phosphate-buffered saline solution (PBS, pH 7.5) was added to the dried reagent to prepare an aqueous solution of [^{125}I]Bolton-Hunter reagent. The reagent solution prepared was impregnated into the gelatin hydrogel sheet at a volume of 20 μl per sheet. The resulting hydrogel sheets were kept at 4°C for 3 h to introduce ^{125}I into the amino groups of gelatin. The gelatin hydrogel sheets radioiodinated were rinsed in DDW, which was exchanged periodically at 4°C for 4 days, to exclude non-coupled, free ^{125}I-labeled reagent from ^{125}I-labeled gelatin hydrogel sheets. When measured periodically, the radioactivity of DDW returned to a background level after 3 days rinsing. No shape change of hydrogel sheets was observed during radiolabeling and the subsequent rinsing process, irrespective of hydrogel preparation conditions.

Estimation of in vivo *degradation of gelatin hydrogels*

In vivo degradation of gelatin hydrogels was evaluated in terms of the radioactivity loss of ^{125}I-labeled gelatin hydrogels implanted. Various types of ^{125}I-labeled gelatin hydrogels were implanted in the back subcutis of ddY mice (3 mice per group, 6–7 weeks old, Shimizu Laboratory Supply, Kyoto, Japan) under pentobarbital anesthesia. At 1, 3, 7, 10, 14 and 21 days after hydrogel implantation, the radioactivity of hydrogels implanted was measured on a gamma counter (ARC-301B, Aloka, Tokyo, Japan). Next, the mouse back skin around the hydrogel implanted site was cut into a strip of 3×5 cm^2 and the corresponding facial site was thoroughly wiped off with a filter paper to absorb ^{125}I-labeled gelatin. The radioactivity of the skin strip and the filter paper was measured to evaluate the remaining radioactivity of tissue around the implanted hydrogel. The ratio of total radioactivity measured to the radioactivity of hydrogel implanted initially was expressed as the percentage of remaining activity for hydrogel degradation. The number of mice in each experimental group was 18, while 3 mice were killed at each time point for *in vivo* evaluation. The half-life time periods of gelatin hydrogels were evaluated from the time-course curve of radioactivity remaining of ^{125}I-labeled gelatin hydrogel. All the animal experiments were done according to the Institutional Guidance of Kyoto University on Animal Experimentation.

Statistical analysis

Experimental results were expressed as the mean ± S.D. (standard deviation of the mean). Graphs were drawn based on the least-square approximation method and the correlation coefficient was described as R^2 value.

RESULTS

Cross-linking density and water content of gelatin hydrogels prepared by different gelatin types and cross-linking methods

Figure 2A and 2B shows the number of cross-links per molecule gelatin of hydrogels cross-linked by GA and dehydrothermal treatments for different time periods. Figure 2C and 2D shows the number of cross-links per molecule gelatin of hydrogels prepared by UV irradiation for different time periods after dehydrothermal treatment for 24 h and different doses of electron beam irradiation. Irrespective of the gelatin type, the number of cross-links per gelatin molecule increased with increasing time of GA and dehydrothermal treatments. The number of cross-links of basis gelatin hydrogels increased with UV irradiation time up to 10 min, but leveled

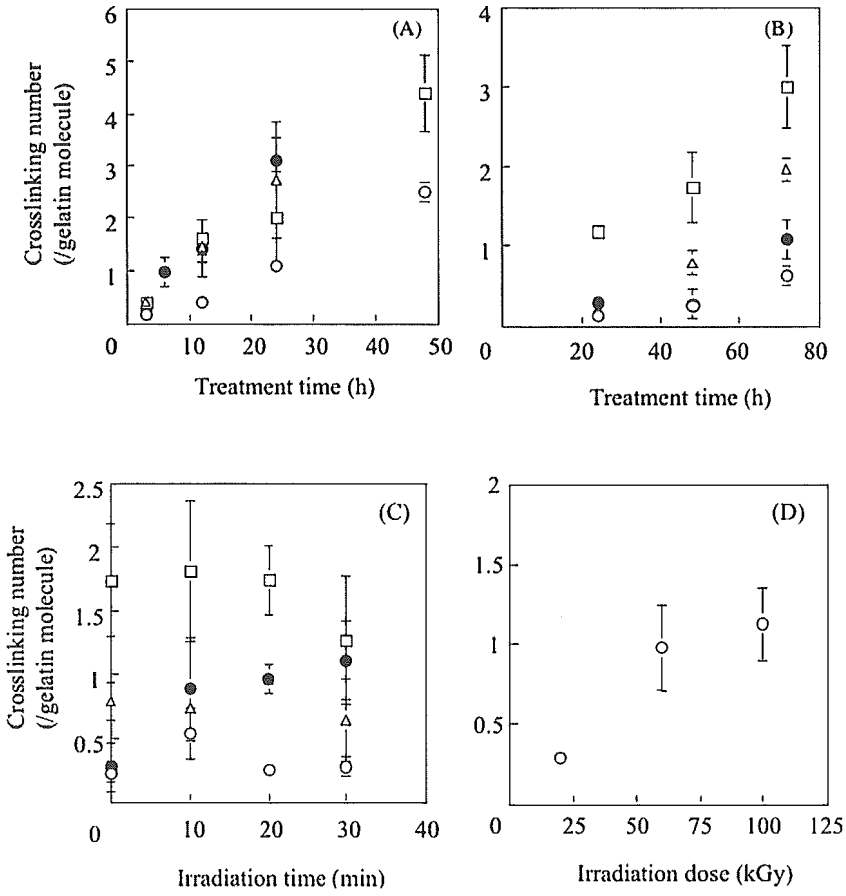

Figure 2. The number of cross-links per gelatin molecule of hydrogels as a function of GA treatment time (A), dehydrothermal treatment time (B), UV irradiation time (C) and electron beam irradiation dose (D). The hydrogels were prepared from acidic gelatin extracted from bovine bone (○), porcine skin (△) or fish scale (□) and basic gelatin extracted from porcine skin (●).

off thereafter. On the other hand, no big influence of irradiation time on the number of cross-links for acidic gelatin hydrogels was observed. The number of cross-links of gelatin hydrogels tended to increase as the irradiation dose increased, although the increment was as large as other cross-linking methods.

Figure 3A and 3B shows the water content of gelatin hydrogels prepared by GA treatment and dehydrothermal treatment. Figure 3C and 3D shows the water content of gelatin hydrogels prepared by UV irradiation after dehydrothermal treatment for 24 h and different dose of electron beam irradiation. The water content decreased with an increase in the time of GA and dehydrothermal treatments. However, the difference of water content between the types of gelatin was bigger than that in the number of cross-links. The water content of gelatin hydrogels rapidly decreased when UV irradiation was done for 10 min, but longer UV irradiation did not

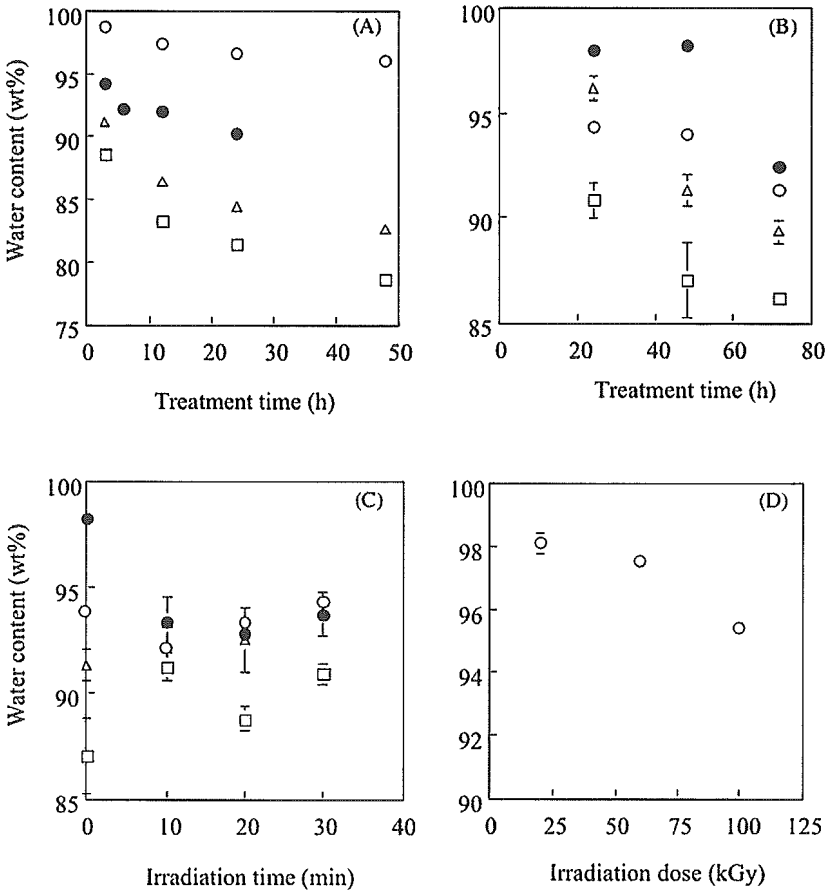

Figure 3. The water content of gelatin hydrogels as a function of GA treatment time (A), dehydrothermal treatment time (B), UV irradiation time (C) and electron beam irradiation dose (D). The hydrogels were prepared from acidic gelatin extracted from bovine bone (○), porcine skin (△) or fish scale (□) and basic gelatin extracted from porcine skin (●).

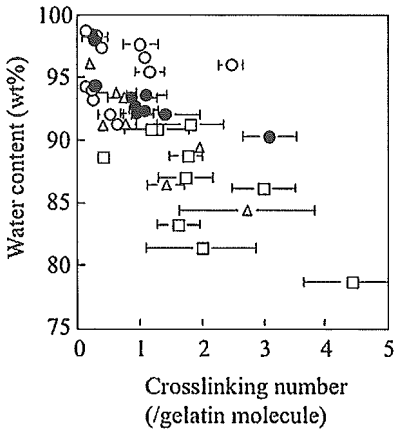

Figure 4. Relationship between the number of cross-links of gelatin molecule of hydrogels and the water content of gelatin hydrogels. The hydrogels were prepared from acidic gelatin extracted from bovine bone (○), porcine skin (△) or fish scale (□) and basic gelatin extracted from porcine skin (●).

contribute to any change in the water content of hydrogels. The water content slightly decreased with the increased dose of electron beam.

Figure 4 shows the relationship between the number of cross-links per molecule gelatin of various hydrogels and their water content. The water content of gelatin hydrogels decreased with an increase in the number of cross-links. This good correlation was observed only for gelatin of the same type. However, the correlation pattern in the water content–cross-linking point relationship was not similar between the different types of gelatin hydrogels.

In vivo *degradability of gelatin hydrogels with different water content and the number of cross-links*

Figure 5 shows the relationship between the water content of hydrogels prepared from each type of gelatin by various cross-linking methods and the hydrogel biodegradability. When compared for the same type of gelatin hydrogels and cross-linking methods, the *in vivo* half-life time of gelatin hydrogel became longer as the water content decreased. However, the correlation of half-life time and water content was different from hydrogel to hydrogel. Figure 6 shows the relationship between the biodegradability of gelatin hydrogels and their number of cross-links. Only hydrogels of fish-scale gelatin, prepared through GA cross-linking, showed slower biodegradability than the hydrogels from other types of gelatin. However, irrespective of the cross-linking methodsand the gelatin type, there was better correlation between the *in vivo* degradability of gelatin hydrogels and their number of cross-links ($R^2 = 0.837$) than that between their degradability and water content ($R^2 = 0.729$).

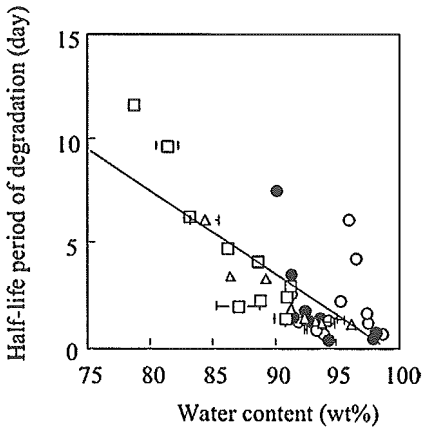

Figure 5. Relationship between the *in vivo* degradation of gelatin hydrogels and water content of the hydrogels. The hydrogels were prepared from acidic gelatin extracted from bovine bone (○), porcine skin (△) or fish scale (□) and basic gelatin extracted from porcine skin (●). The line was drawn based on the least-squares approximation method ($R^2 = 0.729$).

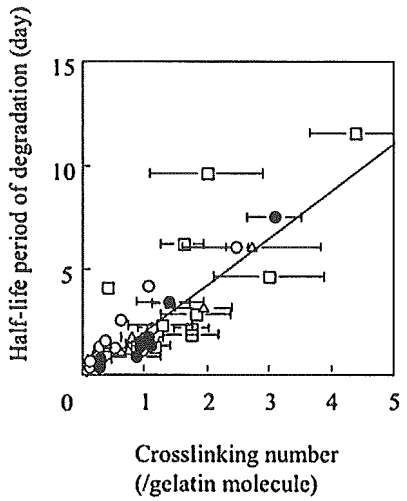

Figure 6. Relationship between the *in vivo* degradation of gelatin hydrogels and the number of hydrogels cross-links. The hydrogels were prepared from acidic gelatin extracted from bovine bone (○), porcine skin (△) or fish scale (□) and basic gelatin extracted from porcine skin (●). The line was drawn based on the least-squares approximation method ($R^2 = 0.837$).

DISCUSSION

In this study, gelatin hydrogels were prepared through different cross-linking methods from various types of gelatin, extracted from several kinds of animal species. The cross-linking density of gelatin hydrogels could be controlled by the time of cross-linking and irradiation. Similar to the water content of hydrogels, the number of cross-links in hydrogels was changed by the conditions of hydrogel preparation.

Gelatin hydrogels were prepared by GA or dehydrothermal treatment and UV or electron beam irradiation. Among the chemical cross-linking agents, GA is most widely used due to its high efficiency in the stabilization of collageneous materials [31]. Cross-linking of collagenous samples with GA involves the reaction of free amino groups of lysine or hydroxylysine residues of polypeptide chains with the aldehyde groups of GA [32]. It is likely that GA can cross-link between the two amino residues of collagen chains. It has been reported that dehydrothermal treatment generates chemical bonding between the amino and carboxyl groups of collagen molecules due to thermal dehydration [33, 34]. Dehydrothermal cross-linking can occur only if the amino and carboxyl groups are close to each other. Thus, it is possible that dehydrothermal treatment allows gelatin molecules to cross-link to a lesser extent than GA treatment. When compared for the gelatin hydrogels cross-linked by GA treatment, the number of cross-links in hydrogels prepared from porcine skin gelatin increased more than that in hydrogels prepared from other types of gelatin. However, when compared for the gelatin hydrogels cross-linked by dehydrothermal treatment, the number of cross-links in hydrogels prepared from fish-scale gelatin was the highest of all. The difference may be due to a difference of the transition temperature. In the case of fish-scale gelatin, the gelatin molecules may be closer to each other because the transition temperature from random coil to helix conformation is higher. The hydrogels prepared from fish-scale gelatin were cross-linked more than other type of gelatin.

It is reported that UV irradiation generates radicals at the aromatic residues of gelatin amino acids, such as tyrosin and phenylalanine. The binding of these radicals will react to each other, resulting in cross-linking formation [34, 35]. However, from Figs 2C and 3C it can be seen that the cross-linking density of gelatin hydrogels largely changed depending on UV irradiation time. When the irradiation time was short, UV irradiation would enable gelatin to cross-link intermolecularly. However, it is possible that irradiation for longer time preferably acts on the chain scission of gelatin molecules. A balance of the cross-linking and chain scission would result in unchanged density of hydrogel cross-linking. This same phenomenon has been reported in the case of UV irradiation to collagen membranes [36].

Electron beam irradiation also produces radicals [37]. The number of cross-links did not change, whereas the water content of gelatin hydrogels deceased, as the dose of electron beam irradiation increased. The number of cross-links was not large and the water content did not decrease very much. This is because the chain scission by the overdose of electron beam also occurs [38].

There are two methods to assess the cross-linking density of hydrogels. One is from the water content of hydrogels. There is one theoretical equation between the water content of hydrogels and the hydrogel density which contains the Flory–Huggins interaction parameter (χ parameter) [38]. Thus, when the cross-linking density is assessed based on water content, the χ parameter is required. The water content of gelatin hydrogels was different between the types of gelatin or cross-

linking methods. It is likely that the χ parameter of gelatin greatly depends on the gelatin type because the amino acid sequences are different among the gelatin samples which are prepared by various treatments (acidic, basic and emzymatic) from collagen of different sites and animals. Although the χ parameter of gelatin is reported to be 0.495 [39], the method to assess the cross-linking density from the hydrogel swelling may be inaccurate. Therefore, in this study, we have chosen to determine the cross-linking density of hydrogels from their tensile modulus [28]. Gelatin hydrogels behave as a rubber-like material. From the stress–strain behavior of gelatin hydrogels swollen, the number of cross-links can be assessed. For this assessment to calculate the cross-linking level of gelatin hydrogels by classical rubber theories, the ideality of chains is basically assumed. In this study, since the strain of hydrogels was small, it is theoretically possible that the hydrogels deform in an entropic modulus manner. When the degree of cross-linking in gelatin hydrogel is lower, hydrogel is so fragile that the tensile test cannot be performed. In that case, the compressive test can be substituted for the tensile test [40]. Therefore, this method is useful to assess the cross-linking density, such as the number of cross-links of gelatin hydrogels.

Mechanical testing and enzymatic degradation of gelatin hydrogel have been performed in the past [41–43]. One paper reported that cross-linked gelatin was degraded in an alkaline protease solution [41]. As that study, some other studies reported only one kind of gelatin type, a few kinds of cross-linking methods and *in vitro* enzymatic degradation. However, this study used various kinds of gelatin types and various kinds of cross-linking methods and performed in the back subcutis of mice.

Gelatin hydrogels are degraded *in vivo* not by simple hydrolysis, but by proteolysis. Therefore, in the present study, several radioiodinated gelatin hydrogels were implanted into the mouse subcutis to evaluate the time profile of hydrogel degradation. We have demonstrated that the time profile of radioactivity remaining in ^{125}I-labeled gelatin hydrogels in the back subcutis of mice was in good accordance with that of hydrogel weight [44]. As shown in Fig. 6, there is a good correlation between the number of cross-links in gelatin hydrogels and the degradability of gelatin hydrogels. This can be explained in terms of susceptibility to protease attack. It is likely that the cross-linking density of hydrogels stereochemically reduces the molecular approach of protease to gelatin chains, resulting in less susceptibilty of hydrogels to proteolysis. The hydrogels prepared through GA cross-linking of fish-scale gelatin were degraded more slowly than other hydrogels (Fig. 6). This may be due to the molecular hydrophobicity of GA and the transition temperature of gelatin. GA is a cross-linker with a hydrophobic moiety of methylene chain. It is well recognized that the transition temperature of fish collagen is higher than that of other animal collagens. Therefore, the fish-scale gelatin is likely to form a helix structure compared with other types of gelatin. Based on this feature, it is possible that the molar percentage of helix–helix interaction of gelatin molecules in the hydrogel of fish-scale gelatin is higher than that of other hydrogels, resulting

in reduced approach of proteases to gelatin chains. In addition, the GA hydrophobicity also suppresses the protease approach to gelatin chains. These natures of fish-scale gelatin, different from gelatin of other animal species, would cause the lower degradability of fish-scale gelatin hydrogels. When the *in vivo* biodegradability of hydrogels is compared by the measure of hydrogel water content, a big dependence of the gelatin type and cross-linking method on the degradation was observed. This implies that the water content is only one measure to express the density of hydrogel cross-linking for one type of gelatin and cross-linking method and not universal. The present study indicates that the biodegradability of gelatin hydrogels can be determined by the number of cross-links per gelatin molecule, irrespective of the gelatin type and cross-linking method.

Acknowledgements

The authors gratefully acknowledge Mr. Fukano and Mr. Ishiguro (Nichiban Co., Ltd., Tokyo, Japan) for preparing gelatin hydrogels cross-linked by electron beam irradiation.

REFERENCES

1. D. L. Stocum, *Science* **276**, 59 (1997).
2. Y. Tabata, *Tissue Eng.* 9, S5 (2003).
3. Y. Tabata and Y. Ikada, *Adv. Drug Deliv. Rev.* **31**, 287 (1998).
4. D. Zekorn, *Bibl. Haematol.* **33**, 30 (1969).
5. N. Chakfe, Y. Marois, R. Guidoin, X. Deng, M. Marios, R. Roy, M. King and Y. Douville, *Polym. Polym. Composit.* **1**, 229 (1993).
6. Y. Marois, N. Chakfe, X. Deng, M. Marois, T. How, M. W. King and R. Guidoin, *Biomaterials* **16**, 1131 (1995).
7. G. A. Digenis, T. B. Gold and V. P. Shah, *J. Pharm. Sci.* **83**, 915 (1994).
8. R. Narayani and K. P. Rao. *J. Biomater. Sci. Polym. Edn.* **7**, 39 (1995).
9. R. Guidoin, D. Marceau, T. J. Rao, M. King, Y. Merhi, P. E. Roy, L. Martin and M. Duval, *Biomaterials* **8**, 433 (1987).
10. R. A. Jonas, G. Ziemer, F. J. Schoen, L. Briton and A. R. Castaneda, *J. Vasc. Surg.* **7**, 414 (1988).
11. Y. Marois, N. Chakfe, X. Deng, M. Morois. T. How, M. W. King and R. Guidon, *Biomaterials* **16**, 1131 (1995).
12. J. Bachet and D. Guilmet, *Cardiol. Clin.* **17**, 779 (1999).
13. J. Bachet and D. Guilmet, *Cardiol. Clin.* **17**, ix (1999).
14. Y. Otani, Y. Tabata and Y. Ikada, *Biomaterials* **19**, 2091 (1998).
15. Y. Tabata, K. Uno, T. Yamaoka, Y. Ikada and S. Muramatsu, *Cancer Res.* **51**, 5532 (1991).
16. P. Kallinteri and S. G. Antimisiaris, *Int. J. Pharm.* **221**, 219 (2001).
17. M. M. Welz and C. M. Ofner, *J. Pharm. Sci.* **81**, 85 (1992).
18. M. Muniruzzaman, Y. Tabata and Y. Ikada, *J. Biomater. Sci. Polymer Edn* **9**, 4593 (1998).
19. A. J. Kuijpers, P. B. van Wachem, M. J. van Luyn, J. A. Plantinga, G. H. Engbers, J. Krijgsveld, S. A. Zaat, J. Dankert and J. Feijen, *J. Biomed. Mater. Res.* **51**, 136 (2000).
20. L. Di Silvio, N. Gurav, M. V. Kayser, M. Traden and S. Downes, *Biomaterials* **15**, 931 (1994).
21. A. Veis, *The Macromolecular Chemistry of Gelatin.* Academic Press, New York, NY (1964).
22. Y. Tabata, S. Hijikata and Y. Ikada, *J. Control. Rel.* **31**, 189 (1994).